

Article

Weather Simulation of Extreme Precipitation Events Inducing Slope Instability Processes over Mountain Landscapes

Alessio Golzio ^{1,*} , Irene Maria Bollati ² , Marco Luciani ³, Manuela Pelfini ² and Silvia Ferrarese ¹ 

¹ Department of Physics, Università degli Studi di Torino, Via Giuria 1, 10125 Torino, Italy; silvia.ferrarese@unito.it

² Earth Sciences Department “A. Desio”, Università degli Studi di Milano, Via Mangiagalli 34, 20133 Milano, Italy; irene.bollati@unimi.it (I.M.B.); manuela.pelfini@unimi.it (M.P.)

³ Studio di Geologia Luciani, Viale Castelli 17, 28868 Varzo, Italy; marco.luciani@geologiapiemonte.it

* Correspondence: alessio.golzio@unito.it

Received: 15 May 2020; Accepted: 16 June 2020; Published: 20 June 2020



Featured Application: High-resolution weather analysis and forecasts for warnings and civil protection against landslides and hydrological instability.

Abstract: Mountain landscapes are characterised by a very variable environment under different points of view (topography, geology, meteorological conditions), and they are frequently affected by mass wasting processes. A debris flow that occurred along the Croso stream, located in the Italian Lepontine Alps in the Northern Ossola Valley, during summer 2019, was analysed from a geological/geomorphological and meteorological point of view. The debris flow was triggered by an intense precipitation event that heavily impacted a very restricted area over the course of three hours. A previous debris flow along the same stream occurred in Autumn 2000, but it was related to an intense and prolonged rainfall event. The slope was characterised in terms of sediment connectivity, and data were retrieved and elaborated from the Web-GIS (Web-Geographic Information System) database of the IFFI-Italian Landslide Inventory and historical archives of landslides. Both the events were analysed through the weather research and forecasting (WRF) model applying a very high horizontal grid spacing with the aim of catching the precipitation patterns and timings. The obtained results are compared with the observed precipitation at a selection of weather stations in the area. The simulation of WRF that measured the timing in total precipitation and in its minor steps could be considered reliable. Moreover, it reveals to be appropriate for detecting in advance the meteorological conditions potentially triggering mass-wasting processes affecting slopes featuring high connectivity conditions and lithotypes characterised by a high Landslide Susceptibility Index.

Keywords: weather simulation; precipitation; WRF; slope instability processes; complex mountain environment; Northern Ossola Valley (Italy)

1. Introduction

Mountain environments are being particularly affected by climate change, especially in terms of water resources and streamflow regimes [1]. In recent times, among water-related geomorphological processes often responsible of alpine landscape evolution [2], mass-wasting events are potentially triggered by climate change, and by extreme events, in particular, that could act at different time scales [3,4]. According to Gariano and Guzzetti [5], the relationship between type, spatial extent, and magnitude of the changes, as well as the location, activity, and frequency of landslides in response

to the projected climate change, are not straightforward. Moreover, the analysis of climate-landslide relation is complicated by the partial overlap on spatial and temporal scales between these two elements [5]. In addition, in the last decades and in the near future, due to the increasing occurrence of heavy and concentrated or prolonged rainfalls [6], mass movements, in particular debris flows, are expected to increase in frequency and/or magnitude [7–9].

The involved meteorological parameters should be investigated and forecasted with specific detail and could reveal to be effective in mitigating risk scenarios deriving from this kind of processes. In this context, the forecasts of meteorological events that trigger this kind of landslide are challenging for two main reasons. Firstly, mountain topography is complex being characterised by high peaks and sometimes narrow valleys that are hardly resolved by orographic input dataset [10]. In order to reach a high-performance model, it is necessary to decrease the vertical and horizontal grid-spacing to fit both the atmospheric physical processes and the narrow valley spaces [10]. For these reasons, the actual mesoscale meteorological models need a high-resolution input dataset for orography, land-cover, soil texture, and vegetation patterns to correctly depict the underlying terrain [11]. These detailed data are necessary as much as the boundary meteorological conditions. Secondly, the meteorological events that can trigger debris flows are characterised by continuous and prolonged rainfall or by intense precipitation in a short period over small geographical areas [12]. Especially in this second case, meteorological forecast models are hardly able to identify the amount of rainfall, their timing, and the limited areas affected by rain.

On the Alps, where complex terrains make the use of high spatial resolutions mandatory in meteorological models, the grid-spacing in meteorological model applications is generally set at a value ranging between 1.0 and 1.5 km, but sometimes it might be not enough [13]. COSMO (CONsortium for Small scale MOdelling) model, operatively used by MeteoSwiss and several universities and environmental agencies for weather forecasts and research purposes, runs at the maximum resolution of 1.1 km over the Alpine arc [14,15], while MOLOCH model, developed at ISAC-CNR (Institute for Atmospheric and Climate Sciences, National Research Council Italy) and covering all Italian peninsula, has been set at the minimum grid-spacing of 1 km [16]. RAMS (Regional Atmospheric Modelling System) has been applied over highly complex terrain, in the Hindu-Kush Karakorum and Himalaya regions, at the maximum resolution of 1 km [17]. The WRF (Weather Research and Forecasting) model [18] is widely used worldwide as a consequence of its open-source distribution, however its default set-up permits the maximum horizontal grid-spacing of 1 km over complex terrains [19,20]. An increased horizontal and vertical resolution could provide useful information about the meteorological processes over complex terrain.

All meteorological models compute the precipitation patterns and their time evolution during the event. These data are fundamental to investigate the meteorological phenomena. Moreover, they can also be used to drive hydrological model systems that can predict the amount of water resources and their fluctuations [21,22]. The desire advance in the actual knowledge is to produce a trustworthy and with a small grid-spacing weather forecast, including precipitation.

At this scope, in the present work, a valley slope in the Northern Ossola Valley (Lepontine Alps) was selected. The Ossola region is characterised by heavy instability phenomena and recurrent debris flow events, due to meteorological conditions coupled with geological features (e.g., widespread loose debris and fractured rocks) and hydrographic basins morphology ([23], and reference therein). Particular attention was paid to the last two debris flow events affecting the Croso stream basin in the Cairasca Valley in 2000 and 2019. Concerning the meteorological background, the 2000 and 2019 events were triggered by different kinds of rainfall episodes. In the first case, prolonged and heavy rainfalls occurred, while during the second one, intense and localised precipitations affected the investigated area. During the most recent one, happened on the 12 August 2019 a series of debris flows affected the slopes of the Cairasca Valley, provoking temporarily interruptions along the Cairasca stream. The local road was also interrupted, fortunately without any casualty. The Croso stream basin was hence characterised also from a morphometric, geological and geomorphological perspective to

understand the predisposing and preparing factors inducing debris flows affecting the slope. In more detail, the investigated slope was analysed from a morphometric point of view, and the Italian Web-GIS based database and historical archives on hydrogeological instabilities were also examined.

The main aim of the present work is analysing the precipitations that triggered the two debris flow events within the Croso stream basin, using the WRF model adequately adapted to work at high-spatial-resolution (500 m of grid-spacing) in mountainous terrain. The WRF meteorological model was set-up as previously tested by [24], and applied to the two episodes. The simulated results were compared with observations at five meteorological stations in the studied area and, finally, related to the geological background of the slope.

2. Study Area

The hamlet of San Domenico (Municipality of Varzo, Verbano-Cusio-Ossola Province, Italy) is located in the Lepontine Alps, in the Piedmont region and in the Ossola Valley, on the North-Western border with Switzerland. The area is part of the Toce hydrographic basin (Figure 1), well known in the literature for its mean climatic conditions [25,26], the geological features (e.g., abundant loose debris and fractured rocks) and hydrographic basin morphology. These latter favour heavy instability phenomena [23,27], among which debris flow events could be recurrent, especially along weakness zones. The most recent instability event that we are focusing on occurred along the Croso stream on the 12 August 2019, when a debris flow interrupted the road connecting the San Domenico village with the Ponte Campo locality. The Croso stream is located within the Cairasca hydrographic basin (basin area: 78.9 km²; perimeter: 46.7 km) part of the Toce hydrographic basin (basin area: 1784.4 km²; perimeter: 291 km). The Cairasca stream is a left-tributary of the Diveria stream and, subsequently, of the Toce river. It is characterised by an intermittent flow. It is 3.7 km long with a mean steepness of 30%. The Croso hydrographic basin (basin area 3.23 km²; perimeter 10.5 km) is characterised by a peak of water discharge of about 22–23 m³/s, with a return time interval of 200 years [28].

The location of the studied slope with the distribution of the meteorological stations is reported in Figure 1.

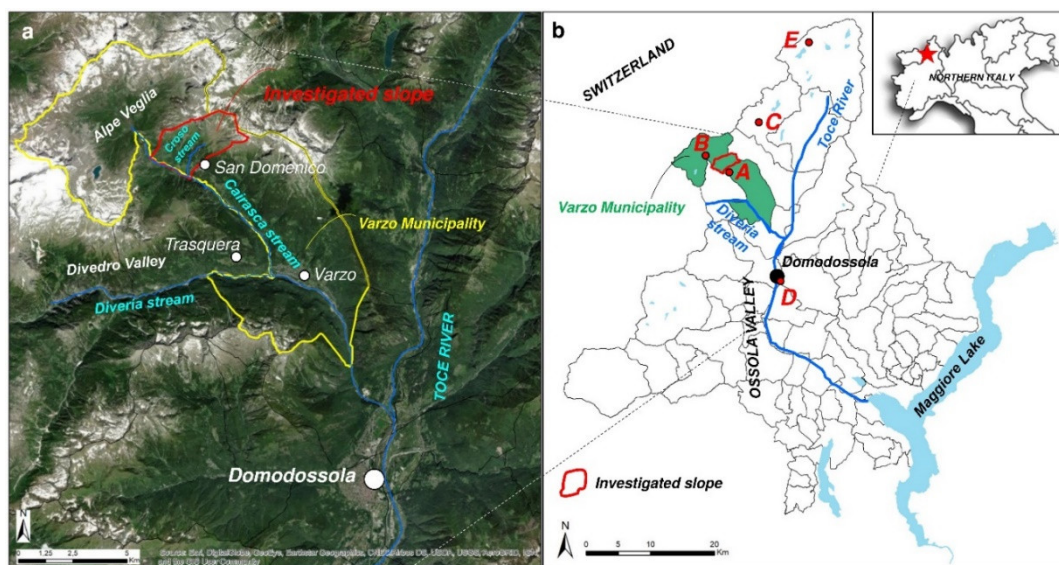


Figure 1. The geographical setting of the study area. (a) The investigated slope within the Cairasca stream hydrographic basin; (b) the investigated slope in the context of the Verbano-Cusio-Ossola province with the distribution of the meteorological stations (see codes and details in Table 1). Background of a: Environmental Systems Research Institute (ESRI) DigitalGlobe & GeoEye (GIS User commonly; <http://microsites.digitalglobe.com/arcgis/>).

Table 1. The weather station positions and their distance from the Croso stream. Measured variables: R, rain; T, temperature; S, snow height; W, wind speed and direction; P, atmospheric pressure; G, global radiation; H, humidity. See locations reported in Figure 1.

Station Name	ID	Latitude N (°)	Longitude E (°)	Altitude (m)	Distance (km)	Instruments
San Domenico (Varzo)	A	46.250	8.193	1308	0.7	R,T
Alpe Veglia	B	46.275	8.146	1736	4.0	R,T,S,W,G,P
Alpe Devero	C	46.316	8.260	1634	9.2	R,T,S,H
Domodossola	D	46.103	8.302	252	19.0	R,T,W,P,G
Formazza	E	46.433	8.358	2453	24.0	R,T,S,W

3. Background of the Event

3.1. The Geological Background and Geomorphological Setting of the Slope

The study area (i.e., the investigated slope in Figure 1a,b) is located in the Central-Western Alps, and more in particular in the Lepontine gneiss dome area, where basement nappes alternate with (meta)sedimentary cover series constituting a NW-verging stack of basement and post-Carboniferous cover nappes [29]. The Barrovian metamorphism of Oligocene to Miocene age, affecting the nappes, varies from upper greenschist to amphibolite facies [30]. The Lower Penninic nappes characterise in particular the investigated slope. They are highly metamorphic crustal nappes representing the former rift shoulder and syn-rift European margin [31]. Along the slope, rocks of the following Penninic Units crop out from SE to NW (Figure 2a):

- Antigorio and Teggiolo Units: they occupy a crucial tectonic position, on the boundary between the Helvetic and Penninic realms [32]. The *Antigorio Unit* is constituted by monzogranitic to granodioritic orthogneiss representing the basement of the series [29,31]. It is overlain by the *Teggiolo Unit*, comprised of several sedimentary cycles, separated by erosive surfaces and large stratigraphic gaps, whose age ranges from Triassic to Eocene [30]. The limit between the two units is locally erosive.
- Valais Unit: they are composed by calcschists deriving from the sediment of the Valais basin, and they are of Cretaceous-Paleogene age [31].
- Lebedun Unit: it is a paragneiss assemblage [30,33] constituted of thick clastic deposits that can be defined as polymictic conglomerate and micaschists. Their age is estimated as Cretaceous [29]. They are interpreted as former syn-rift deposits [31].

The area underwent glacial modelling during the Pleistocene Age, when at the Last Glacial Maximum (26.5–19 ka; [34]) the extension of the Toce glacier reached the area down-valley the Maggiore Lake, flowing into the nearby Ticino Glacier, and contributing in building the Lake Maggiore glacial amphitheatre [35]. In correspondence of the Simplon Pass, at the head of the Divedro Valley, a transfluence saddle was present [35], allowing the flow of Swiss Rhône ice dome into the Toce one. The Cairasca hydrographic basin is characterised, up-valley to the study area, by the glaciostructural depression of the Alpe Veglia, bordered by the reliefs where now glaciers are still present [36]. The Alpe Veglia area is then connected with the Cairasca Valley bottom through a deep gorge, the Cairasca Gorge, carved into Lebedun paragneiss and carbonatic rocks of the Valais Unit, and along which instability processes often occur. The study area, SW exposed, is located along the left hydrographic side of the Cairasca valley, and it is up-slope characterised by a low steep accumulation area where [37], in correspondence of the Alpe Ciamporino ski area, glacial deposits related probably to a Holocene glacial stage are present. The basin is surrounded by scree slope deposits at the base of the Pizzo del Dosso ridge. Down-slope, the edge of the Alpe Ciamporino terrace, the steepness increases, interrupted by the presence of minor terraces. Signs of the water- and gravity-related processes are evident and dominantly characterise the deglaciated areas. Moreover, a series of NE-SW oriented quite vertical

fractures is present, conditioning the direction of some streams that deeply incise the slope and along which debris flows are recurrent. Hence the hydrography of the area is mainly controlled by structures, lithology and morphological elements, as in other areas in the Ossola region [38]. Recent land-use features are reported in Figure 2b (Corine Land Cover 2012-IV level): the slope is characterised in the upper part by more or less continue grasslands and by broadleaves and coniferous forests in the middle and lower slope. The main human settlements in the area, representing potentially vulnerable spots, are the San Domenico hamlet and the San Domenico Ski area at the Alpe Ciamporino, and the road network. The hamlet and the ski area are located on terraces and are popular both during winter, for skiing, and during summer for excursionists since they represent the most popular access to the Alpe Veglia and Devero Natural Park. In Figure 2c, the Hillslope model shows the two sub-basins characterising the investigated portion of the slope with the evident incision of the Croso stream recurrently affected by debris flows.

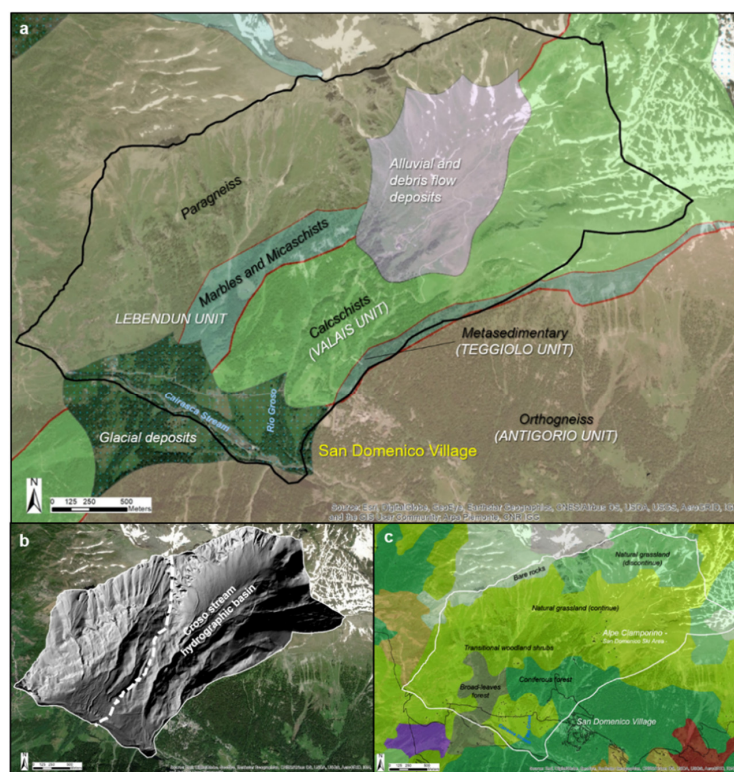


Figure 2. The investigated slope nearby the San Domenico hamlet and the Alpe Ciamporino ski area. (a) Geological map (source ARPA Piemonte layers; geologia e dissesto, 1:250,000; source https://webgis.arpa.piemonte.it/Geoviewer2D/index.html?config=other-configs/geologia250k_config.json); (b) Hillslope model elaborated from a DTM of 5 m of resolution (source <http://www.geoportale.piemonte.it/cms/>); (c) Corine Land Use 2012–Level IV (source Geoportale Nazionale; <http://www.pcn.minambiente.it/mattm/servizio-wms/>); Background courtesy of Environmental Systems Research Institute (ESRI) DigitalGlobe & GeoEye (GIS User commonly; <http://microsites.digitalglobe.com/arcgis/>).

3.2. Meteorological Background

The synoptic meteorological situation between 10 and 13 August 2019 was characterised by a low surface pressure (995 hPa) moving North from Ireland to Norway related with a high troposphere trough from Northern Atlantic Ocean (Iceland) to France. The axis of the trough was rotating eastward, and a cold front passes the Alps on the 10 August (Figure 3a). This front caused sparsely distributed showers on the Lepontine Alps and Northern Ossola Valley. The mean wind from 700 hPa to 300 hPa was from West-South-West. The satellite images on North Italy showed thin clouds, comparable to

small afternoon thunderstorms, in fact, the Figure 3e does not indicate deep convection, and the type of clouds is low and middle (Figure 3g).

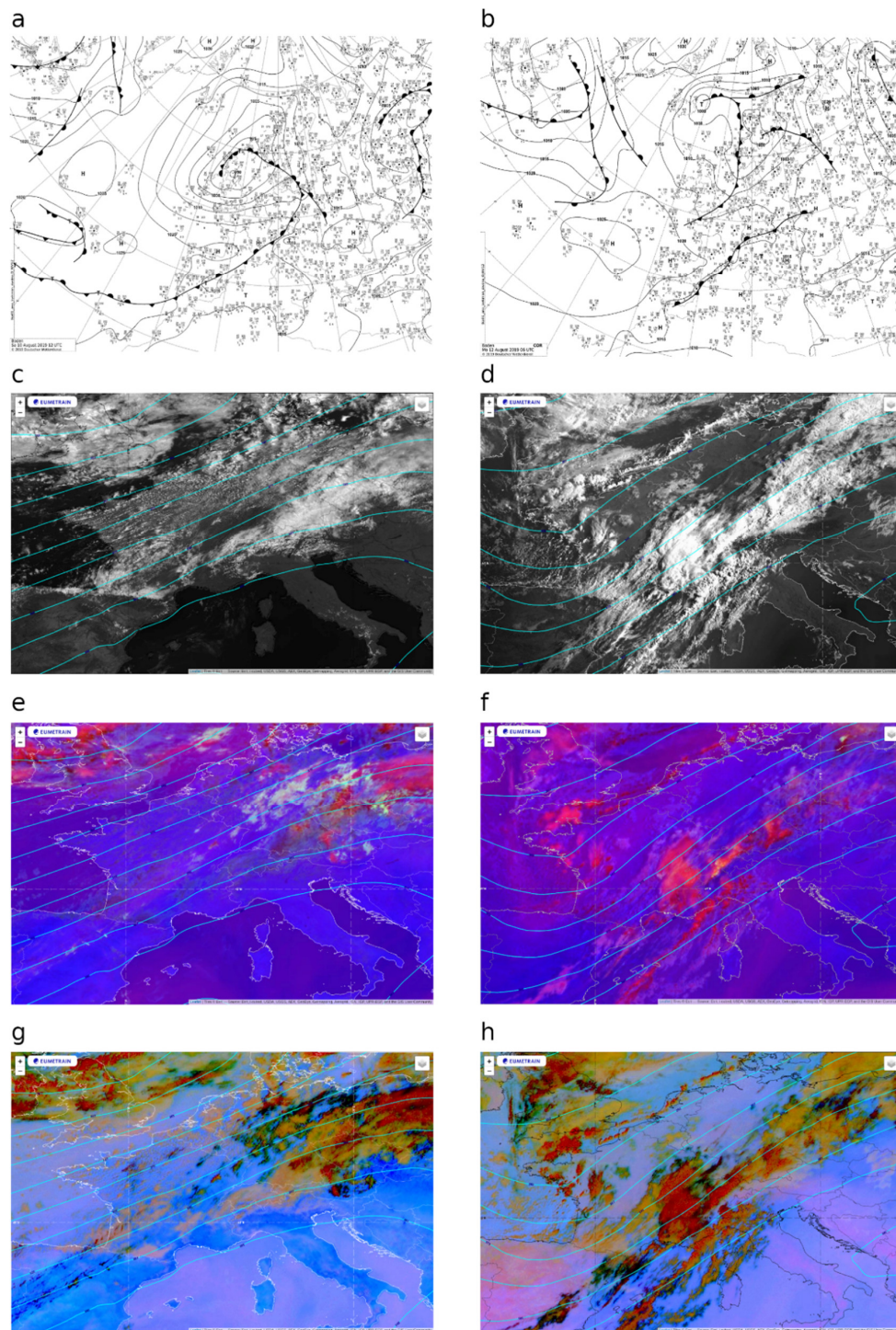


Figure 3. (a,b) Surface pressure chart analysis, with station data, fronts and isobars; (c,d) satellite HRV (High-Resolution Visible) image; (e,f) satellite RGB convection-enhanced product (red and orange indicate high convection); (g,h) satellite RGB Dust product (yellow: low clouds; green: middle clouds; black-dark red: high clouds; red: convective clouds). Blue lines on satellite images represent geopotential heights at 500 hPa in decametres. Left panels (a,c,e,g) refer to Saturday 10th August 2019 at 1200 UTC, while right panels (b,d,f,h) refer to Monday 12th August 2019 at 0600 UTC. Source DWD Archive for panels a and b, Eumetrain for satellite images.

After this first passage, only low clouds persisted over the investigated area for the following 36 h, when the progressive expansion of a high-pressure field from the Azores Islands modified the mean flow to South-West and increased the instability over the Po Valley. During the 11th afternoon, a huge thunderstorm was registered between Novara and Milano, and it vanished before the Ossola Valley. The changed circulation advected warm and moist air from the Mediterranean Sea over the Western Alps and Apennines and generated a stationary front that insisted on the Alps between 0600 UTC and 1200 UTC of the 12 August (Figure 3b). The maximum cloud cover was reached between midday and afternoon when the most intense precipitation was registered on the neighbouring plains (Novara, Vercelli and Milano) and piedmont areas. This front caused the precipitation that between 0600 UTC and 0620 UTC provoked the debris flow along the Croso stream. Between 10 and 13 August the maximum Convective Available Potential Energy (CAPE) measured at Milano Linate sounding occurred on 12 August (1200 UTC, 2282 J/kg), indicating the most unstable conditions among all these days. However, Milano Linate is roughly 120 km distant from the studied area, and its profile could be only partly representative. The deep convection located on Ossola Valley at 0600 UTC on 12 August is well depicted in the satellite RGB products (Figure 3f); afterwards, the cloudiness expands towards entire Piedmont, Aosta Valley and Lombardy regions (i.e., North-Western Italy), and it moved towards East during the afternoon.

Fair weather conditions characterised the following days. The weather conditions were also deduced with the several webcams in the San Domenico area, and with the global radiation measured at the Alpe Veglia station (B in Figure 1; Table 1).

The last meteorological event that caused the activation of the Croso stream debris flow dated back to October 2000, when a flood affected entire North-Western Italy. In this case, the precipitation lasted for four days, from the 11 to the 17 October 2000. The precipitation type was totally different from the 2019 event, in fact, it was characterised by steady rain, with a mean rain-rate of 2–3 mm over ten minutes (roughly 12–20 mm/h), averaged over the five weather stations.

The core of this flood was concentrated between Friday 13th and Monday 16th October, when a cyclonic area was generated on Great Britain Islands and a pronounced trough elongated from North to the Iberian Peninsula. A high-pressure ridge on Eastern Europe promoted the block of the frontal zone on Western Europe and the Alps.

A South-South-West, and subsequently a South-East advection brought warm and moist air on Piedmont region from the Mediterranean Sea. The baroclinicity of this situation enhanced the convergence on the Western Po Valley and the Western Alps, causing the concentration of precipitation from the Alps down to the Piedmont plain.

In the following days, a cold-drop was generated from the previous trough and slowly moved towards the French Coast; this situation favoured the stationarity of the frontal zone on Piedmont and the moist advection from the Mediterranean Sea. On Sunday 15th, a second depression moved towards the North and triggered the formation of thunderstorms on plains, due to the saturated air related to the decreasing of temperature on the region.

The event ended in the night of Monday 16th, when the Azores Anticyclone progressively expanded over Western Europe [39].

4. Methods

4.1. The Characterisation of the Croso Stream Slope

In order to characterise the Croso stream debris flow, the production of thematic maps on sediment connectivity, the analysis of the hydrogeological instabilities archives, and the calculation of the parameters useful to comprehend the magnitude of the event were performed.

- (i) Elaboration of the thematic maps on sediment connectivity: Sediment Connectivity is the degree of linkage (lateral, longitudinal, and vertical) that controls sediment fluxes throughout landscape [40]. Sediment Connectivity Index (IC), was calculated according to Cavalli et al. [40] (<https://github.com>).

[com/HydrogeomorphologyTool](#)), since it is a topographic based approach addressed to assess the lateral connectivity, specifically, for small mountain catchments. The IC calculation (1) considers the: (i) upslope component (Dup), i.e., the potential for downward routing of the sediment produced upslope; (ii) downslope component (Ddn), that takes into account the flow path length that a particle has to travel to arrive at the nearest target or sink. The two components consider the surface roughness (w), the average slope gradient (s) and the upslope contributing area (a). The sediment connectivity is calculated considering the Log10 of the ratio between the upslope and downslope components for the sediment flux with a target that could be the outlet of the basin or, more specifically, as done in this case, the channel network. Using channel network as a target is more indicated if the aim is the comparison with specific geomorphic features along a slope [41]. As suggested by the Authors, we used a high-resolution Digital Terrain Model-DTM (5 m resolution, source Geoportale Regione Piemonte; <http://www.geoportale.piemonte.it/cms/>).

$$\text{Index of Connectivity (IC)} = \log_{10}\left(\frac{Dup}{Ddn}\right) \quad (1)$$

where $Dup = \overline{WS} \sqrt{A}$ and $Ddn = \sum_i \frac{d_i}{w_i s_i}$.

- (ii) Analysis of the Web-GIS and the related database of the Italian Landslide Inventory (Progetto IFFI, ISPRA–Istituto Superiore per la Protezione e la Ricerca Ambientale; <http://www.progettoiffi.isprambiente.it/cartografia-on-line/>). This database has been migrated in 2020 to the new IdroGEO platform (<https://idrogeo.isprambiente.it/app/>; CC BY SA 4.0). The IFFI project is aimed at realising the inventory of the landslides affecting the Italian territory according to photointerpretation, historical archives, past projects analyses, and field survey. The Web-GIS and the related database of the IFFI Project [42,43] include the landslide that can be mapped at a 1:25000 scale, i.e., those characterised by a volume of at least 10000 m³. The spatial resolution is of 5 m, and the metric precision is of 12.5 m. The IFFI database has already been used within specific analyses on the susceptibility of slopes to landslides [44], where more variables were taken into account. In addition to basic information (level I forms), “IFFI second level forms”, including, bedrock condition, damages, monitoring and risk scenarios have been retrieved for the Croso stream basin. The information was also derived from the Arpa Piemonte-SIFraP (Sistema Informativo Frane in Piemonte <http://webgis.arpa.piemonte.it/Web22/webgis/sifrap.zip>). Data were finally integrated with historical archive analyses [28] and were put in relation with the IC map (i).
- (iii) Calculation of the morphometric and kinetic parameters. This kind of parameters are useful to provide an idea about the magnitude of the event. The calculation of the volume of the debris accumulated on the alluvial fan after the 12 August 2019 event was derived from a rough approximation. Three sections were considered: (i) the last overwhelmed check-dam, (ii) the closure section at the overwhelmed bridge on the stream; (iii) an intermediate section. The sections were compared before and after the debris flow event and the final value was obtained using the average value between the surfaces comprised among the sections and the distance between these sections. Moreover, the debris flow velocity was roughly calculated in this framework, according to the time lag between the last passage of car drivers before the debris flow event occurred, and the debris flow overwhelming the bridge (i.e., 10 min). The length of the stream was hence divided by this time interval. These data were finally integrated with the data from the Radarsat, ERS and ENVISAT derived from the IFFI database (“IFFI second level” forms) and reported as indicated in the SIFraP database.

4.2. Weather Station Network and Simulation Set-Up

The precipitations that caused the Croso stream debris flow on 12 August 2019 was measured by five weather stations in the area, managed by ARPA Piemonte (Agenzia Regionale per la Protezione dell’Ambiente, Environment Protection Agency). The distribution of the weather stations is reported in

Figure 1b, and the full description of these stations is reported in Table 1. The closest one to the Croso stream is the San Domenico pluviometric station, located at the central square of the same name hamlet. The distance between this station and the Croso stream bridge, overwhelmed by the debris flowing during the analysed events, is 0.7 km. The Alpe Veglia (where a long-term campaign is studying the micrometeorology [45]) and the Alpe Devero stations are situated, respectively, on the North-Western and Northern sides of the Croso stream basin, and they are respectively 4.0 km and 9.2 km away from the Croso stream. Domodossola and Formazza stations are respectively 19 and 24 km far from the Croso stream.

The weather data are available every 10 min for the precipitation values (accumulated rain in 10 min), while the other variables are available on 30 to 60 min intervals.

In parallel with the analysis of weather station data, a simulation with the mesoscale WRF model (Weather Research and Forecasting model, version 4.1.2 [18]) was performed for both the events (2000 and 2019). The set-up of the model had been previously tested over other Alpine regions [24] and applied here. The model was run on ECMWF ERA5 reanalysis boundary conditions (European Centre for Medium-Range Weather Forecast) [46], and three two-way nested domains were considered (4.5 km, 1.5 km and 0.5 km of grid-spacing) with 61 vertical levels up to 90 hPa (Figure 4). The topography is given by the NASA SRTM 3 arc-second DEM (Digital Elevation Model, [47]) and the land-cover by the Corine Land Cover database (2012; [48]). The parametrised options were microphysics WSM6 scheme [49,50] shortwave scheme with orographic shading, RRTM longwave scheme [51], MM5 surface layer revised scheme [52], Noah land surface model [53], YSU boundary layer scheme [54] with topographic wind drag option, cumulus Grell and Freitas ensemble scheme [55] activated on the parent domain only.

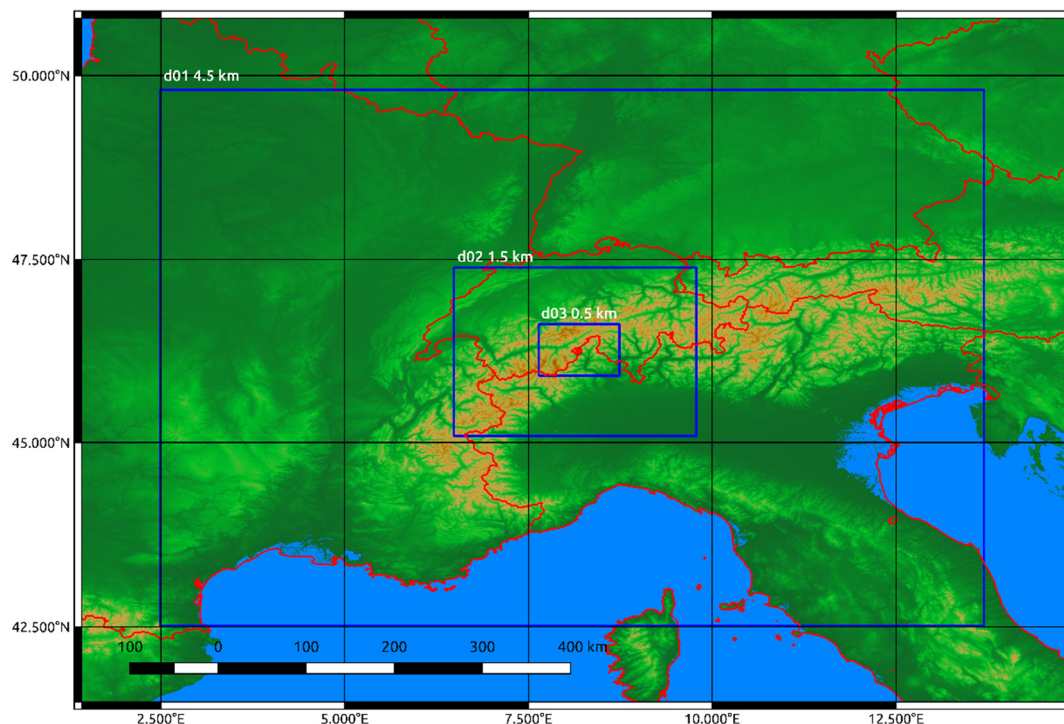


Figure 4. The WRF simulation domains (in blue) with the topography from NASA SRTM DEM used for the WRF preprocessing system.

The comparison between observations and model outputs was performed on the station locations and considering the areal distribution of precipitations. The distribution of stations was chosen with the aim of testing the performance of the WRF model to predict the event, and the closest ones were chosen to quantify the amount of rain triggering the debris flow directly.

5. Results and Discussion

5.1. The Characterisation of the Croso Stream Slope

In Figure 5, the results of the index of connectivity map elaboration (a), and of the IFFI database analyses (b) are reported.

Table 2. Landslides located along the investigated slope and included in the IFFI database (*Activity degree codes*: A = Active; R = Reactivates; S = Suspended; Q=Quiescent; n.d. = not determined; *Landslide classification codes*: D-Rf/F = Diffuse rockfall/toppling; Rf/T = Rockfall/toppling; DSGD = Deep Seated Gravitational Deformation; C = Complex; E/Df = Earth/Debris flow; *Lithology*: Lp = Lebendun paragneiss; Lm-ms = Lebendun marble and micaschists; Vc = Valais calcschists; Ao = Antigorio ortogneiss; *Land Use codes (CLC Corine Land Cover 2012 Level IV)*: Ng = Natural grassland; Bt = Broadleaves trees; Cf = Coniferous forest; *IFFI Method codes*: P = Photointerpretation; Ha = Historical archives). The Croso stream incision affected by debris flows is depicted in bold characters.

ID (Figure 5b)	IFFI Idfrana	IFFI Sub-Id	Landslide Classification	Activity Degree	Lithology (Arpa Piemonte 1:250,000)	Land Use	IFFI Method	Area (m ²)
1	10300266-	00	D-Rf/T	A7R/S	Lp	Ng	P	41562
2	10300267-	00	D-Rf/T	A/R/S	Lp	Ng	P	8880
3	10300271-	00	Rf/T	Q	Lp	Ng	P	52058
4	10300274-	00	Rf/T	Q	Lp	Ng	P	48159
5	10300275-	00	Rf/T	Q	Lp	Ng-Bt	P	47248
6		01	DSGD	n.d.	Lp-m-ms, Vc, Ao	Ng-Bt-Cf	P	1892974
7		02	C	Q	Lp	Ng	P	200507
8		03	E/Df	Q	Vs	Ng-Cf	P	116899
9		04	E/Df	Q	Ao	Cf	P	5534
10		05	E/Df	Q	Lm-ms, Vc	Ng	P	20161
11	10300484-	06	E/Df	Q	Lm-ms, Vc	Ng	P	21952
12		07	E/Df	Q	Lm-ms	Ng	P	1528
13		08	E/Df	Q	Lm-ms	Ng	P	5945
14		09	C	Q	Lm-ms	Ng	P	3779
15		10	D-Rf/T	A/R/S	Vc	Ng-Cf	P	5860
16		11	D-Rf/T	A/R/S	Vc	Ng-Cf	P	11262
17	10300497-	07	D-Rf/T	A/R/S	Ao	Cf	P	58294
18	10310431-	00	D-Rf/T	A/R/S	Lp	Br-Ng	Ha	739041
19	10350258-	00	E/Df	n.d.	Vs	Cf	Ha	9018

The structure of the Croso stream hydrographic basin is clear in terms of sediment connectivity in Figure 5a, where the Index of Connectivity map is reported. In the IC map the distinction between the areas characterised by low connectivity (green) and the area characterised by high connectivity (red) is evident. A high connectivity area is represented by the head of the Croso stream basin where several debris transport channels intersect the detachment niches of diffuse rockfalls/topplings (18, Figure 5b and in Table 2). Low connectivity areas correspond to the accumulation areas that act like a sink, as the terrace on which the Alpe Ciamporino is located. From this area, towards down-valley, the high connectivity conditions recur and concentrate along minor streams and small V-shaped valleys located in correspondence of weakness zones (e.g., 8, Figure 5a, Table 2). Hence, the debris stored within the Alpe Ciamporino sink is transported along the Croso stream, together with the debris produced along the incision, along the Croso stream during the heavy rainfall events. At the confluence with the Cairasca stream, debris flow events feed the alluvial fan (Figure 5a).

According to the IFFI database, the structure of the slope is quite articulated and characterised by different kinds of geomorphological instabilities as reported in Figure 5a and Table 2. As mentioned before, up-valley to the study area, the Cairasca gorge is deeply incised as attested to by the intense erosive action of the Cairasca stream, which the Croso stream flows into.

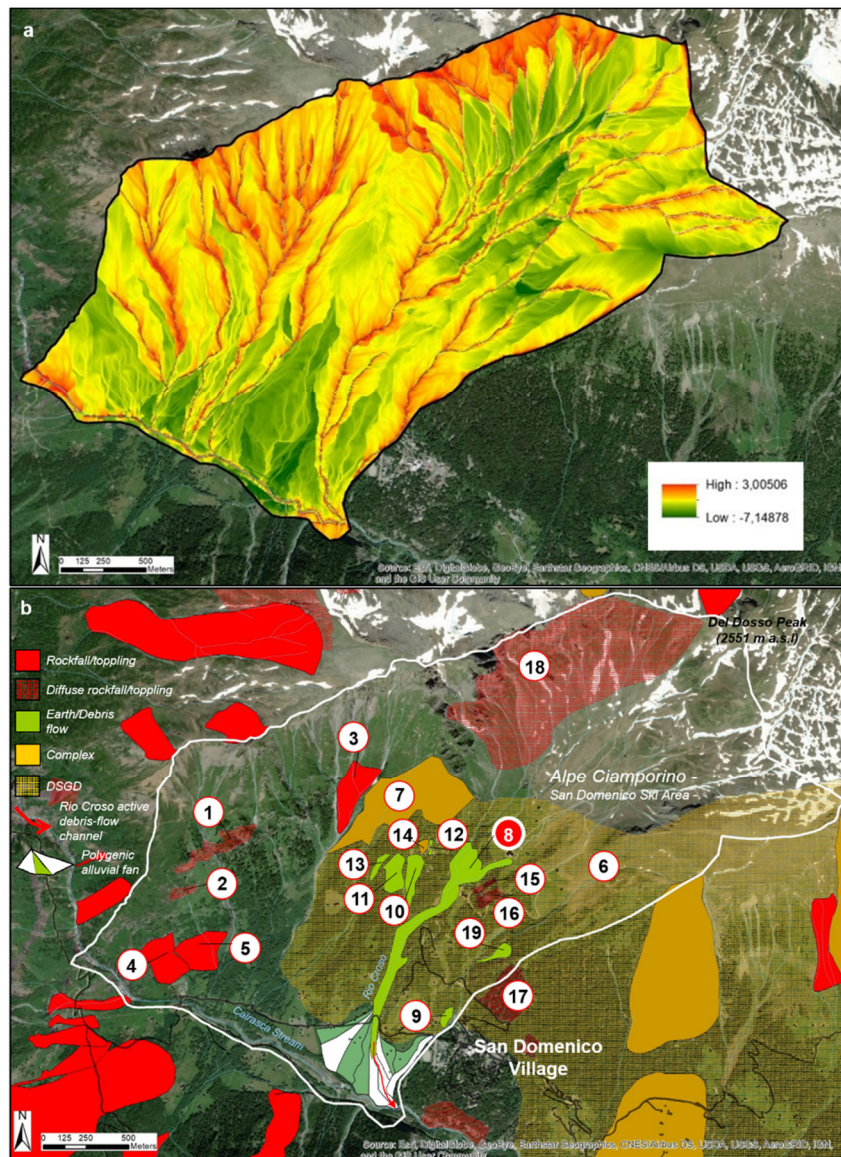


Figure 5. Sediment connectivity and hydrogeological instabilities within the Croso stream basin. (a) the *Index of Connectivity* map with channel network as target elaborated according to [40] using the DTM 5 m resolution; (b) the alluvial fan (source <http://webgis.arpa.piemonte.it/geoportale/>) and landslides retrieved from the WMS of the IFFI–Italian Landslides inventory (source <http://www.progettoiffi.isprambiente.it/cartografia-on-line/> recently moved to <https://idrogeo.isprambiente.it/app/>) (for numbers refer to Table 2). Background courtesy of Environmental Systems Research Institute (ESRI) DigitalGlobe & GeoEye (GIS User commonly; <http://microsites.digitalglobe.com/arcgis/>).

According to IFFI and SIFraP sources ([29,43] and later review), in the Piedmont Region, at least 1230.8 km² (4.8% of the territory) are exposed to Hazard 3 and Hazard 4 categories. The most recent data (2020) include, in the whole Piedmont region, a record of 36787 inventoried landslides of which 3553 (9.66%) are slow earth/debris flow movements and 3859 (10.49%) are fast earth/debris flow movements, as those occurring within the Croso stream hydrographic basin (8–13; 19 in Table 2). The calcschists represents the lithotype characterised by the highest Landslide Susceptibility Index (>35%) of the whole Piedmont territory [56]. In the IFFI system, the nested-to-each-other landslides are grouped according to a main ID (2nd column; Table 2), but the single landslide body could be distinguished using the sub-ID (3rd column; Table 2). In general, along the investigated slope there are landslides related to different typologies: A1) simple geometry landslides that can be mapped

with a proper polygon, because wider than 10000 m³ (1–5; 17–19, Figure 5a; Table 2); B1) complex geometry landslides that, as mentioned before, can be connected each other by a common factor and that are distinguished by using the sub-ID (6–16, Figure 5a; Table 2). As in this case, the Deep Seated Gravitational Deformation (DSDG; 6 in Table 2) is combined with other types of landslide.

In Table 3, the analysed debris flow is categorised with the IFFI ID 10300484-03 (8 in Figure 5a). It is part, together with others (6–16 in Figure 5a), of a complex system including related to the DSGD (6 in Table 2) and involving a significant part of the slope where the San Domenico village is built. The analysed debris flow incision is located within the stripe of calcschists of the Valais Unit (Vc in Table 2 Figure 2a), foliated carbonate rocks quite degraded that, as mentioned before, are characterised, at a regional level, by the highest Landslide Susceptibility Index [56]. More in detail, along the stream a fault puts in contact the orthogneiss (Ao in Table 2), in a very foliated facies, on the left hydrographic side, with the carbonate facies of the Lebedun Unit (Lm in Table 2), on the right hydrographic side. Along the stream, cataclasites rocks are recurrent, representing a potential weakness zone. Moreover, the detachment niche is located at the edge of the glacial terrace of the Alpe Ciamporino (Figure 6b), where a thickness of several meters of glacial deposits covered by continue natural grasslands are present. Here, the dendritic pattern of the stream changes into a single channel stream that incises the glacial deposits making them unstable and contributing to the feeding of the debris flow. The Croso stream debris flow is the only landslide occurrence along the investigated slope that is provided of a “IFFI second level” form. It is classified in the IFFI system as quiescent, since the processes may undergo reactivation in a short time, in this morphoclimatic context. The effects of the intense meteorological events are very significant also in relation to the presence of abundant loose and unstable debris, representing the predisposing factor. It is a self-feeding process, since during the events, additional material along the thalweg and along the lateral slopes is mobilised too (Figure 6a). Moreover, debris contributions derive from the nearby Fontana stream, an incision draining the slope very close to the San Domenico village. The Croso debris flow is hence classified as a complex, hyper-concentrated flow, possibly extremely rapid (velocity > 5 m/s; [57]) flowing potentially for 600 m of altitude difference. At the confluence with the Cairasca stream, an alluvial fan, characterised by 20–25% of steepness, has generated (Figure 5a). Potentially, the interruption of the Cairasca stream could occur due to alluvial fan accretion. Along the stream, human interventions like check dams for mitigating the risk are present, but during the major events they are often overwhelmed by debris.

Table 3. Hydrogeological instability and mass wasting events affecting the Croso stream and the tributary Fontana stream, located immediately westerly to San Domenico village, before the 2000 event [28].

Date	Typology	Causes	Affected Stream or Slope Portion	Effects
19–20 August 1958	Rapid debris flow	Intense meteorological event	Fontana stream	
16 June 1979	Rapid debris flow	Intense meteorological event	Croso stream Fontana stream	Erosion along the thalweg (up to 10 m) and the lateral scarps between 1440 and 1600 m a.s.l.; damages to a check dam at 1600 m a.s.l. Incision and morainic deposits flow at 1500 m a.s.l.; damages to the aqueduct of San Domenico and to the check dam at 1600 m a.s.l. A landslide at 1400 m a.s.l. involving a surface of 1100 m ² partially obstructed the Fontana streambed nearby the recharge basin of the municipality aqueduct and the electric line.
1 January 1993	Slide	Intense meteorological event	Fontana stream	
20 August 1996	Rock fall		Slope behind San Domenico village	
26 May 1997	Flood		Croso stream and Fontana stream	Erosion along the thalweg and damages to the check dams
7 July 1997	DSGD with diffuse mass wasting episodes		The entire slope	The slope portion interested by active DSGD is of 3.0×10^6 m ³



Figure 6. The Rio Croso hydrographic basin before the event of the 12 August 2019—(a) the Croso stream in 2006 with the very evident steepness and abundant debris; (b) the incision within the terrace of the Alpe Ciamporino; (c,d) the Croso stream after the October 2000 event (see details in Figure 7).

Concerning the historical archive analyses [28], the hydrogeological instability and mass wasting events that occurred along the investigated slope and around the San Domenico village before 2000, are reported in Table 3.

The first event analysed in this research, that activated recently along the Croso stream incision, affecting the down-valley road, dates back to 13–16 October 2000 (Table 3). During the 2000 event, mass wasting, river incision and lateral erosion processes affected extensively the whole Po hydrographic basin. In the adjoining Divedro Valley, for example, the intense and prolonged rainfalls induced, among the others, a landslide causing 15 casualties [58]. The Cairasca Valley was deeply affected by soil slips and debris flows, among which the Croso and Fontana stream debris flow was the most relevant in the area (Figure 6c) and rapid debris flow induced erosion along the thalweg, and damages to check dams and the road.

The second, more recent, event occurred on the 12 August 2019 when a series of debris flows affected the slopes of the Cairasca Valley, provoking temporarily interruptions along the Cairasca stream. Along the Croso stream incision, the most powerful one occurred, whose effects were similar to those registered in 2000 (Figure 7). The videos recorded immediately after the event using a drone is retrievable on the web (courtesy of <https://www.localteam.it>) at <https://www.youtube.com/watch?v=OCPLi63CHxQ>. The bridge, slightly damaged, was completely overwhelmed and filled below with the debris and the organic material, mainly wood (Figure 7a,b). The debris flow was also accompanied by earth flows expanding on lateral pastures (Figure 7c). The road was temporarily closed, having some

consequences on the access to Alpe Veglia, especially because the event occurred during the touristic season. The calculated volume of the debris accumulated on the alluvial fan after the 12 August event is of 37759 m³ (Table 4) and the calculated velocity is of 10.8 km/h (3 m/s). After the 2019 event, a series of interventions were put in place: (i) cleaning of the road and the check dams from the debris; (ii) regulating and collecting the water flow along specific directions on the slope; (iii) positioning lateral defenses along both the stream scarps. Potential future interventions may be addressed to re-profiling the thalweg of the Croso stream and to strengthen the longitudinal and transversal defense works along the stream. In Table 4, the data from the Radarsat, ERS and ENVISAT are reported as indicated in the SIFraP database, together with morphometric data and volumetric data of the last event. The interferometric data show relatively low displacement values, both positive (backward respect to the sensor) and negative (towards the sensor), confirming the sudden nature of this kind of events.



Figure 7. The 12 August 2019 debris flows event along the Croso stream—(a) The bridge covered and filled in below by debris flow accumulation (view taken from the drone video, see along the text); (b) a particular of the left-hydrographic side deviation of the Croso stream active channel (see Figure 6c); (c) view of the earth flows starting down-stream respect to the bridge (view taken from the drone video, see along the text); (d) the up-stream conditions of the Croso stream bed with abundant disrupted deposits (view taken from the drone video, see along the text) (see Figure 6d); (e) a check dam, upstream to the bridge, overwhelmed by debris (see Figure 6c).

Table 4. Rio Croso morphometric data and morphometry of the alluvial fan including the estimation of the debris volume after the 12 August 2019 event. The presented information include original data and data retrieved from IFFI and Arpa Piemonte-SIFraP-Sistema Informativo Frane in Piemonte. Interferometric data (ERS for the time interval 1993–2001; RADARSAT for the time interval 2003–2009; ENVISAT for the time interval 2003–2010) for the Croso stream (from Arpa Piemonte-SIFraP Sistema Informativo Frane in Piemonte). Line Of Sight (LOS); Permanent Scatter (PS); Distributed Scatterer (DS).

Rio Croso Morphometric Data		Alluvial Fan Measure at the 12 August 2019 Event					
Crown altitude Q_c (m)	1925	Area (m^2)	1800	Length (m)	6445		
Toe altitude Q_t (m)	1366	Section	Area (m^2)	Distance (m)	Volume (m^3)		
Horizontal length HL (m)	1890	Bridge	162	1009	29321		
Altitude difference H (m)	620	Lower	376	39	8438		
Slope S ($^\circ$)	18.2	Check dam	60	83	10249		
Total area A (m^2)	116899	Upper	187	72	6710		
Width W_i (m)	40		Total volume (m^2)		37759		
Interferometric Data							
DATASET	Moving velocity along the Line of Sight (LOS) (mm/year)			n° PS/DS	n° PS	n° moving PS/DS	ratio [%]
	Min	Max	Mean				
RADARSAT_asce_nord	−0.69	0.31	−0.23	4	1	0	0
ERS_summ_desce	−1.1	−1.1	−1.1	0	1	0	0
pst_ENVISAT_desce	0.52	0.52	0.52	0	1	0	0

5.2. The Simulated Precipitation

WRF simulated precipitation fields were computed during the two meteorological events (12 August 2019 and 13–16 October 2000) that triggered the investigated mass wasting events. The performance of the predictive system is evaluated by comparison with observations at the weather stations in the investigated area (Table 1). The October 2000 and August 2019 meteorological events, as examined above (Section 3.2), were very different: the first one was characterised by a long-lasting, continuous and diffuse precipitation, while the second one was related to a short-timed, intense and extremely localised precipitation. The difficulties in predicting the second event could be much higher due to the short duration and the small spatial localisation that request high-spatial resolution and a well-tuned convection scheme.

The 12th August 2019 event was simulated by WRF (Figures 8 and 9). In particular, the precipitation patterns (Figure 8) reflect the cold front shape and localises the position of the maximum of precipitation on a small area, including the investigated slope. The precipitation fields showed that the principal rain event occurred at the station sites in one hour and half, from 0600 UTC to 0730 UTC. The rain gauges network (Table 1) confirms the duration of the principal event.

Moreover, in a further inspection of observations versus simulated rain rate at the station locations (not shown), it is clear that WRF caught the time of each peak, with some very small time-shift. In particular, the most intense rain rate (13.6 mm in 10 min) was registered at 0610 UTC (12 August 2019) at San Domenico village, while WRF predicted 10 mm, 15 min later at the same site.

Considering the progressive cumulated rain during the event at the five stations (Figure 9 panels A–E), WRF was able to identify the timing of the episode occurred at all station sites and it simulated correctly also the timing of the two moderate precipitation events that occurred on 10 and 11 August. The precipitation quantity was underestimated of about 20 to 50 mm at all stations with the exception of Alpe Veglia (Figure 9B) where the simulated precipitation was overestimated of 10 mm. In this specific event the high spatial variability of precipitation related to the mountainous terrain was evident. In fact, the precipitation at Alpe Veglia station, that suffered of orographic shadowing by peaks on North-North-West side, was overestimated by WRF due to imprecise and smoothed model topography; meanwhile, the precipitation amounts at all the other stations were underestimated due to some imprecision in the determination of lee-slope convection. Between 0500 UTC and 0700 UTC at San Domenico, the precipitation was 61.4 mm, with a mean hourly rain rate of 30.5 mm.

This precipitation quantity, that activated the Croso basin debris-flow, was predicted by WRF only with 15 min of delay with the value of 25.0 mm and hourly rain rate of 12.5 mm. In this case the cumulated rain was twice as much of the quantity predicted by WRF, and, as aforementioned, the convection scheme (acting at the first domain) and the microphysics scheme had underestimated the lee-side convection and convergence with the South-Alpine airmass. The adoption of a double-moment scheme for the microphysics could partially enhance the performance, even if in other cases that did not change the amount of rain considerably. The planetary boundary layer (PBL) scheme, instead, could be decisive, improving the turbulence, the fluxes, and the PBL convection.

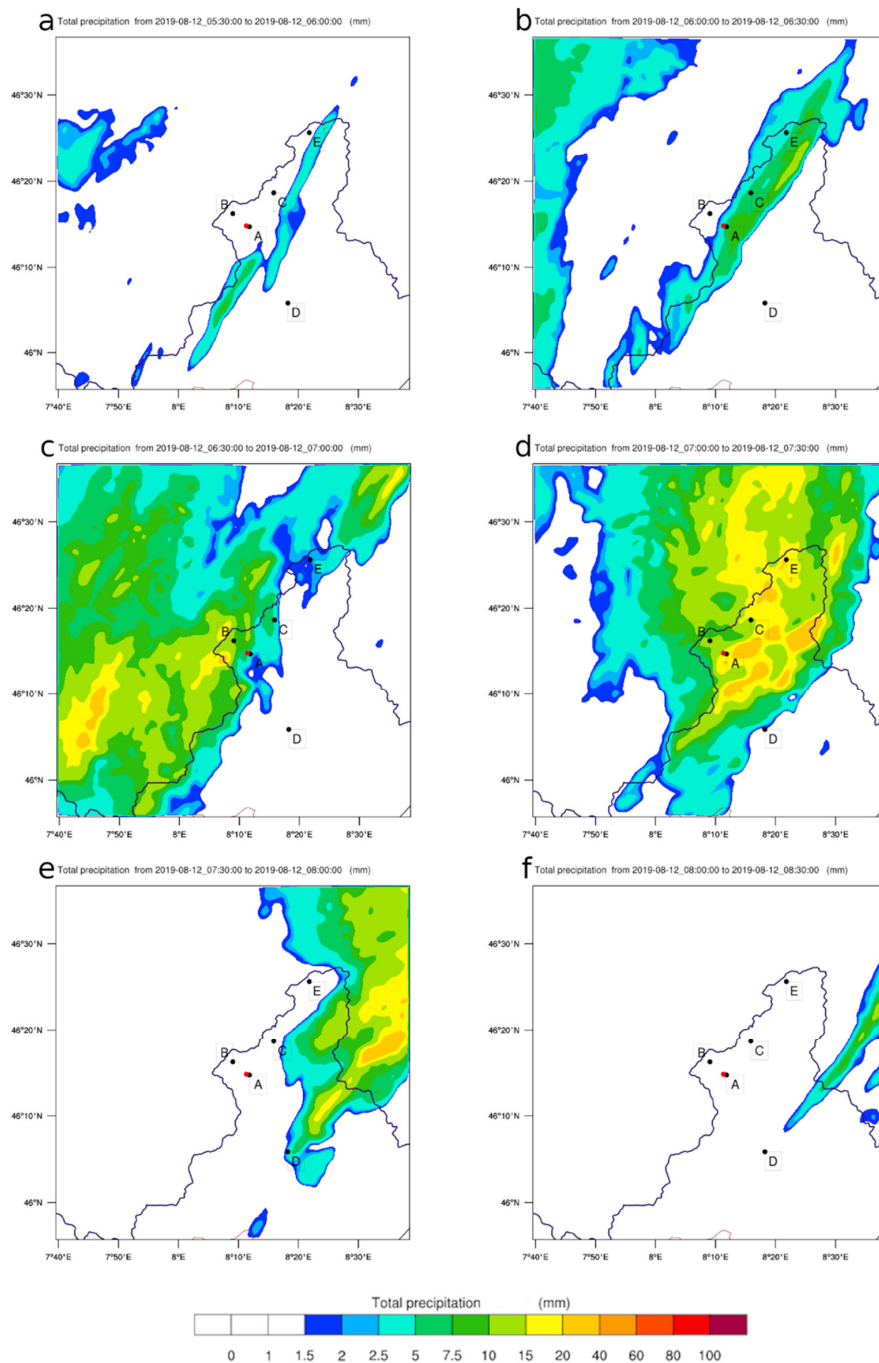


Figure 8. The 12 August 2019 precipitation event simulated with WRF, precipitation totals in 30 min from (a) 0530 UTC to (f) 0800 UTC at 30 min step. Black dots with letters are the locations of weather stations (see Table 1), while the red dot indicates the position of the bridge on the Croso stream.

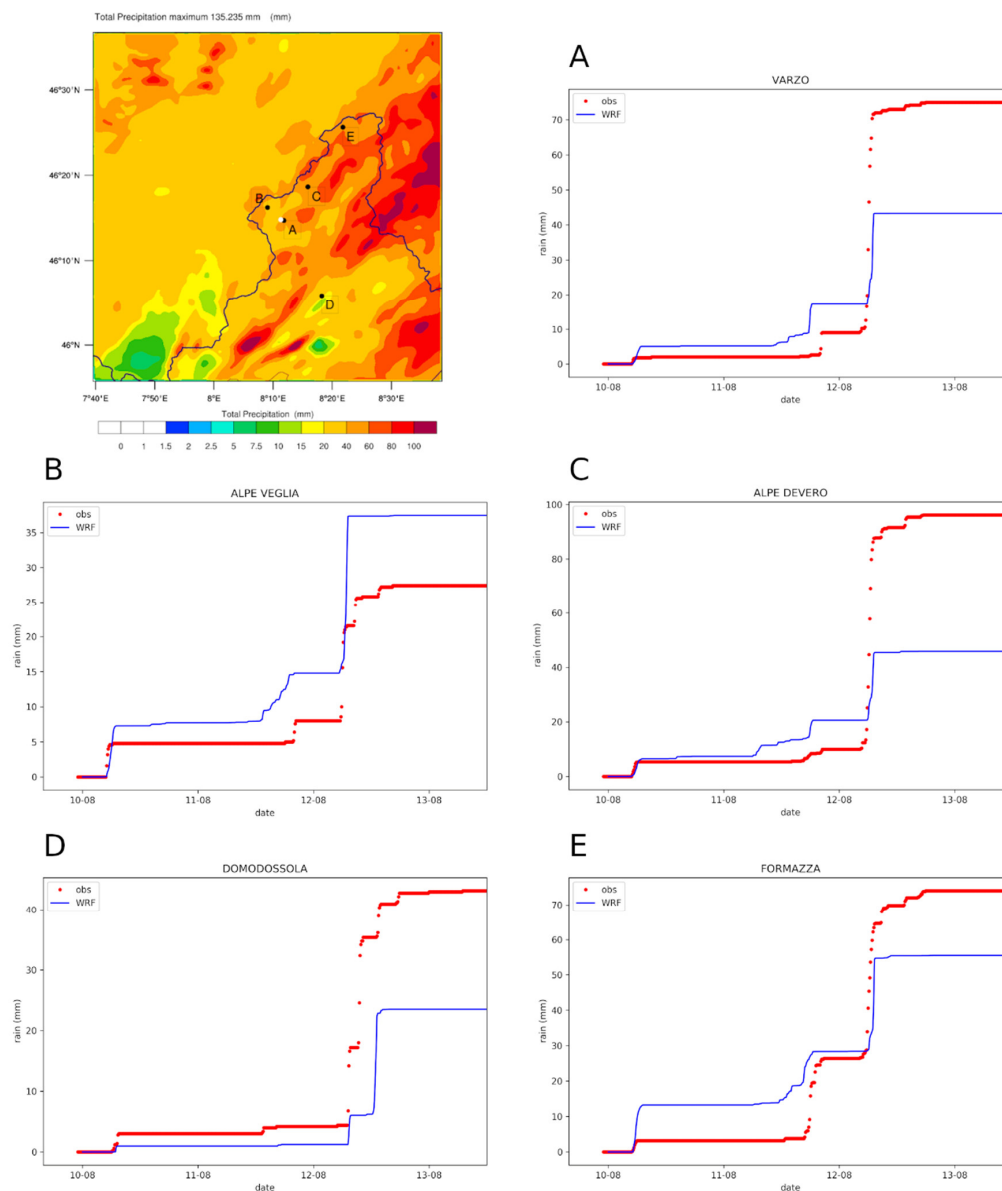


Figure 9. Comparison of simulated (blue lines) and observed (red dots) precipitations at station locations. The top-left panel represents the total simulated precipitation during the period 10 to 15 August 2019. Letters of panels and on the cumulated precipitation plot refer to Table 1. The white dot on the upper left panel indicates the position of Croso stream bridge.

After the peak of 12 August morning, the rainfall stopped, and the totals ranged between 96.2 mm at Alpe Devero and 27.4 mm at Alpe Veglia (first panel in Figure 9). The maximum rainfall predicted by WRF was located easterly, near Locarno (Switzerland), some peaks (greater than 100 mm) at Valle Anzasca and Antrona (South of the study area), and some other peaks (between 80 and 100 mm) along the main Ossola Valley.

From Figure 9 emerges that the WRF was able to catch the timing in total precipitation and also in its minor steps. This is a very important aspect that can allow a realistic forecast of the meteorological conditions triggering mass wasting processes affecting slopes, where high connectivity conditions are verified and lithotypes characterised by a high Landslide Susceptibility Index outcrop.

The August 2019 event was preceded by a relatively long period of slope stability and without prolonged or intense rainfalls, while the slope instability event on the same basin occurred in October 2000. This latter affected the whole North-Western Italy also inducing river floods. The precipitations

measured at the same locations, except Alpe Veglia that was installed on 2 August 2002, reveal the continuous nature of this event that rained from the 11 to the 16 October.

Analysing the station observations, the maximum rain rate over ten-minute intervals, was 9.2 mm at Domodossola (at 1650 UTC on 13 October 2000), while at the other stations it ranged between 3.0 mm (at Formazza) to 8.8 mm (at San Domenico). The mean rain rate over 10 min intervals of the entire event (six days) ranged between 0.3 mm at Formazza to 0.6 at San Domenico.

The cumulated precipitations over the entire event (six days) ranged from 354.8 mm at Formazza to 677.8 mm at San Domenico (Figure 10), so the average precipitation was from 60 to 120 mm per day.

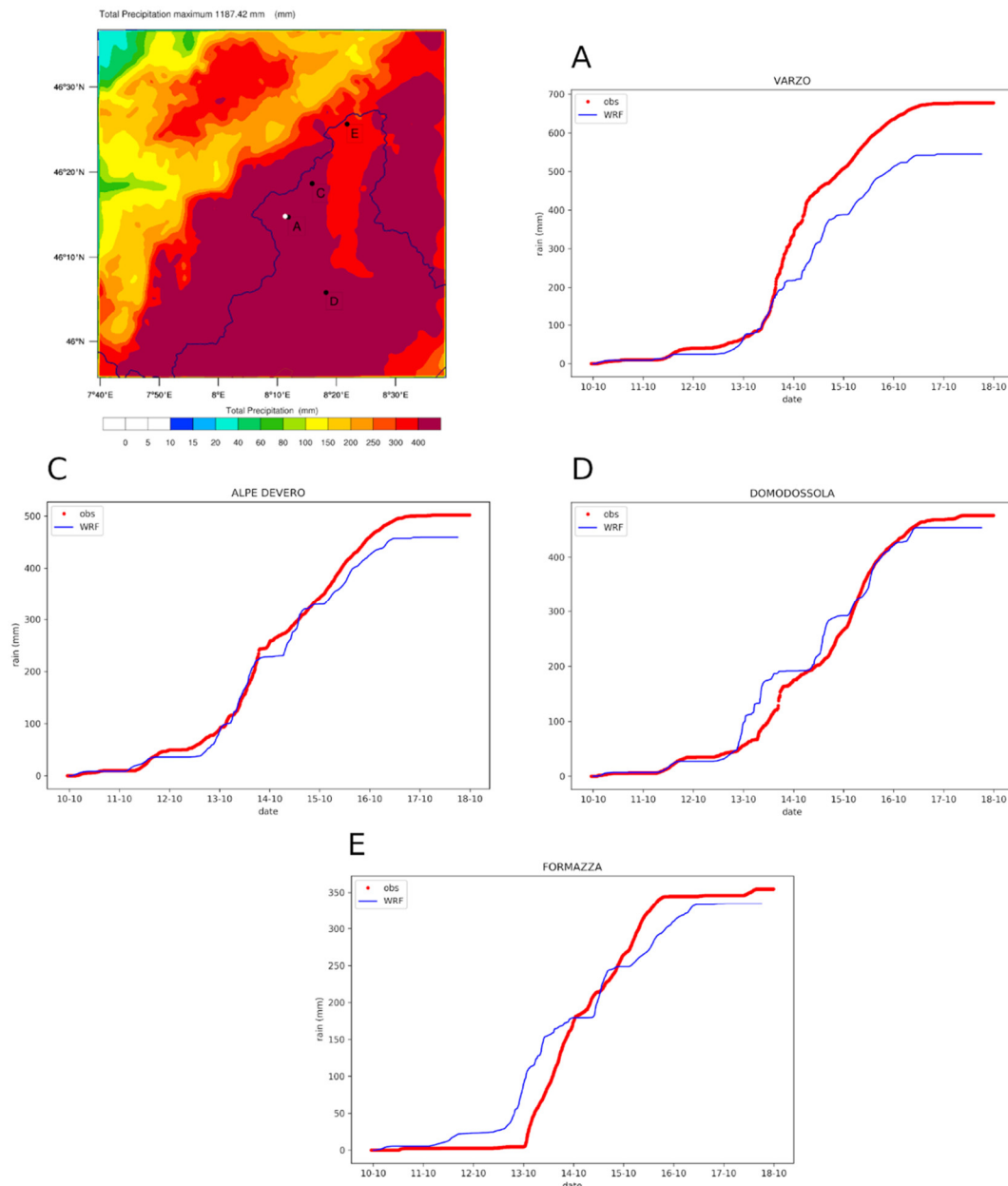


Figure 10. Comparison of simulated (blue lines) and observed (red dots) precipitations at station locations. The top-left panel represents the total simulated precipitation during the period 11 to 17 October 2000. Letters of panels and on the cumulated precipitation plot refer to Table 1. The white dot in the upper-left panel indicates the position of Croso stream bridge. The Alpe Veglia station was not yet installed.

WRF forecasted the event quite well (Figure 10), catching the timing as well as the total precipitation at station locations. The more significant discrepancy was registered at San Domenico (Figure 10A), where WRF simulated 544.9 mm (difference of 132 mm). Meanwhile, the best performance of WRF was registered at Domodossola, where the discrepancy was 22.3 mm. Even with the high-spatial-resolution of the applied WRF set-up, the obtained discrepancies at San Domenico station during the October 2000 event highlight the very high complexity of this site and suggest the importance of a widespread analysis that should also consider the neighbouring areas and the general pattern of precipitation.

In this simulated event, San Domenico station is partly sheltered by the mountains with respect to south-easterly advection. Again, the resolved topography compromised the simulation results, even if the discrepancy between observed and simulated precipitation was only 20% while in August 2019 was 60%.

The up-left panel in Figure 10 shows that the total precipitation simulated by WRF was entirely above 400 mm with a small area characterised by values comprised between 300 and 400 mm.

The relative discrepancy between observed and simulated values are lower during the October 2000 episode rather than during August 2019 one, as a consequence of the meteorological event that, in this second case, is easily captured by WRF. The main difficulties of WRF in mountainous terrain lie in the localisation and description of the convection, and for this reason, the less convective event (October 2000) was better simulated.

6. Conclusions

Debris flow events potentially affecting the Croso stream basin, could be triggered by different kind of meteorological events: prolonged rainfalls episode (i.e., October 2000) or intense and concentrated rainfalls (i.e., August 2019). Despite this, debris flows are characterised by a similar magnitude. The meteorological conditions were computed using WRF model at high horizontal and vertical resolution, in order to capture local phenomena occurring in very complex terrains. The proposed set-up of WRF was able to predict sufficiently well the total precipitation accumulated in the two events, with better performances during the October 2000 event, when floods affected the Piedmont region, and in general the Po plain area. Instead, in August 2019, the total amount of precipitation was in general underestimated by 20 to 50 per cent.

On the other side, in both cases, the timing of the precipitation was correctly predicted by WRF and this aspect reveals the trustworthiness of the actual WRF set-up, that lack only in the intensity of convective processes, but not in the triggering phenomena of precipitation events. The low simulated quantity of precipitation during the August 2019 convective events was probably due to the microphysics scheme adopted (single moment, WSM-6), and probably a double moment scheme could enhance the total amount in case of shallow and deep convection.

The WRF model here applied to a complex slope considering the different kinds of landslides affecting it (Figure 2), has been already applied in the same set-up in different complex mountain terrains [24] and could be adopted to produce the meteorological fields for and a hydrological model that could give an insight into the link between debris flows and precipitation triggering. Moreover, the application of the data coming from the applied WRF model, set with the tested parameters, specific for this kind of terrain, could be an aid within the early warning procedures related to the incoming possibility of specific meteorological events potentially triggering instability events in sensitive areas, like the analysed hydrographic basin. In this context, geological and geomorphological analyses and maps [40] surely contribute to improving knowledge useful to understand the environmental responses to heavy rains better (e.g., rainfall thresholds triggering debris flows; [23,59]) and to investigate hazard and risk scenarios. Moreover, reliable meteorological conditions forecast, together with simplified geomorphological maps and sketches (e.g., Geobox, [2]), could help in spreading knowledge for local management purposes, favouring practices of usable science aimed at mitigating risk scenarios [60].

Author Contributions: Conceptualisation, A.G., I.M.B., M.P., and S.F.; methodology, A.G., I.M.B., and S.F.; software, A.G.; validation, A.G., I.M.B., M.L., and S.F.; formal analysis, A.G.; investigation, A.G., I.M.B., M.L., M.P., and S.F.; data curation, A.G., I.M.B., and M.L.; writing—original draft preparation, A.G., I.M.B., M.L., M.P., and S.F.; writing—review and editing, A.G., I.M.B., M.L., M.P., and S.F.; visualisation, A.G. and I.M.B.; project administration, M.P.; funding acquisition, S.F., M.P., and I.B. All authors have read and agreed to the published version of the manuscript.

Funding: This research is part of the METALP Project, funded by Fondazione CRT, grant 2019.0455; Fondi Potenziamento della Ricerca, Università degli Studi di Milano, linea 2, 2018–2019 (entrusted to I.M. Bollati).

Acknowledgments: The weather station data are retrieved from the ARPA Piemonte weather network database (ANTARES) under the agreement between the University of Turin, department of Physics. Authors are also thankful to Ente di Gestione delle Aree Protette dell'Ossola, Municipality of Varzo, Adolfo and Stefano Zanola supporting the installation of the Alpe Veglia weather station.

Conflicts of Interest: The authors declare no conflict of interest.

References

- Beniston, M.; Stoffel, M. Assessing the impacts of climatic change on mountain water resources. *Sci. Total Environ.* **2014**, *493*, 1129–1137. [[CrossRef](#)]
- Bollati, I.; Pellegrini, M.; Reynard, E.; Pelfini, M. Water driven processes and landforms evolution rates in mountain geomorphosites: Examples from Swiss Alps. *Catena* **2017**, *158*, 321–339. [[CrossRef](#)]
- Soldati, M.; Borgatti, L.; Cavallin, A.; De Amicis, M.; Frigerio, S.; Giardino, M.; Mortara, G.; Pellegrini, G.B.; Ravazzi, C.; Surian, N.; et al. Geomorphological evolution of slopes and climate changes in Northern Italy during the Late Quaternary: Spatial and temporal distribution of landslides and landscape sensitivity implications. *Geogr. Fis. Din. Quat.* **2006**, *29*, 165–183.
- Keiler, M.; Knight, J.; Harrison, S. Climate change and geomorphological hazards in the Eastern European Alps. *Philos. Trans. R. Soc. A Math. Phys. Eng. Sci.* **2010**, *368*, 2461–2479. [[CrossRef](#)] [[PubMed](#)]
- Gariano, S.L.; Guzzetti, F. Landslides in a changing climate. *Earth-Sci. Rev.* **2016**, *162*, 227–252. [[CrossRef](#)]
- Beniston, M.; Stephenson, D.B.; Christensen, O.B.; Ferro, C.A.T.; Frei, C.; Goyette, S.; Halsnaes, K.; Holt, T.; Jylhä, K.; Koffi, B.; et al. Future extreme events in European climate—An exploration of regional climate model projections. *Clim. Chang.* **2007**, *81*, 71–95.
- Crozier, M.J.; Glade, T. The frequency and magnitude of landslide activity Crozier, M.J.; Mausbacher, R. (Eds.), *Magnitude and Frequency in Geomorphology. Z. Geomorphol. Suppl.* **1999**, *115*, 141–155.
- Borgatti, L.; Soldati, M. Hillslope processes and climate change. In *Treatise on Geomorphology: Mountain and Hillslope Geomorphology*; Stoffel, M., Marston, R.A., Eds.; Elsevier: Amsterdam, The Netherlands, 2013.
- Pelfini, M.; Santilli, M. Frequency of debris flows and their relation with precipitation: A case study in the Central Alps, Italy. *Geomorphology* **2008**, *101*, 721–730. [[CrossRef](#)]
- Lehner, M.; Rotach, W.M. Current Challenges in Understanding and Predicting Transport and Exchange in the Atmosphere over Mountainous Terrain. *Atmosphere* **2018**, *9*, 276. [[CrossRef](#)]
- Jiménez-Esteve, B.; Udina, M.; Soler, M.; Pepin, N.; Mirò, J. Land use and topography influence in a complex terrain area: A high resolution mesoscale modelling study over the Eastern Pyrenees using the WRF model. *Atmos. Res.* **2018**, *202*, 49–62. [[CrossRef](#)]
- Crosta, G.B.; Frattini, P. Rainfall-induced landslides and debris flows. *Hydrol. Process. Int. J.* **2008**, *22*, 473–477. [[CrossRef](#)]
- Chow, F.K.; Schär, C.; Ban, N.; Lundquist, K.A.; Schlemmer, L.; Shi, X. Crossing Multiple Gray Zones in the Transition from Mesoscale to Microscale Simulation over Complex Terrain. *Atmosphere* **2019**, *10*, 274. [[CrossRef](#)]
- Schmidli, J.; Böing, S.; Fuhrer, O. Accuracy of simulated diurnal valley winds in the Swiss Alps: Influence of grid resolution, topography filtering and land surface datasets. *Atmosphere* **2018**, *9*, 196. [[CrossRef](#)]
- Goger, B.; Rotach, M.W.; Gohm, A.; Fuhrer, O.; Stiperski, I.; Holtzlag, A.A.M. The Impact of Three-Dimensional Effects on the Simulation of Turbulence Kinetic Energy in a Major Alpine Valley. *Bound.-Layer Meteorol.* **2018**, *168*, 1–27. [[CrossRef](#)]
- Buzzi, A.; Davolio, S.; Malguzzi, P.; Drofa, O.; Mastrangelo, D. Heavy rainfall episodes over Liguria of autumn 2011: Numerical forecasting experiments. *Nat. Hazards Earth Syst. Sci.* **2014**, *14*, 1325–1340. [[CrossRef](#)]

17. Balanzino, A.; Trini Castelli, S. Numerical experiments with RAMS model in highly complex terrain. *Environ. Fluid. Mech.* **2018**, *18*, 357–381. [[CrossRef](#)]
18. Skamarock, W.C.; Klemp, J.B.; Dudhia, J.; Gill, D.O.; Liu, Z.; Berner, J.; Wang, W.; Powers, J.G.; Duda, M.G.; Barker, D.M.; et al. *A Description of the Advanced Research WRF Model Version 4*; NCAR/TN-556+STR; NCAR: Boulder, CO, USA, 2019.
19. Bolla, S.; Branca, M.; Cassardo, C.; Ferrarese, S.; Notarpietro, R. Testing of WRF parametrizations with X-band radar data in a convective rainfall event. *Ital. J. Agrometeorol.* **2017**, *2*, 13–24.
20. Roşu, I.-A.; Ferrarese, S.; Radinschi, I.; Ciocan, V.; Cazacu, M.-M. Evaluation of different WRF parametrizations over the region of Iaşi with remote sensing techniques. *Atmosphere* **2019**, *10*, 559. [[CrossRef](#)]
21. Yu, Z.; Lakhtakia, M.N.; Yarnal, B.; White, R.A.; Miller, D.A.; Frakes, B.M.; Barron, E.J.; Duffy, C.; Schwartz, F.W. Simulating the river-basin response to atmospheric forcing by linking a mesoscale meteorological model and hydrologic model system. *J. Hydrol.* **1999**, *218*, 72–92. [[CrossRef](#)]
22. Jasper, K.; Gurtz, J.; Lang, H. Advanced flood forecasting in Alpine watersheds by coupling meteorological observations and forecasts with a distributed hydrological model. *J. Hydrol.* **2002**, *267*, 40–52. [[CrossRef](#)]
23. Bollati, I.; Lenz, B.C.; Golzio, A.; Masseroli, A. Tree rings as ecological indicator of geomorphic activity in geoheritage studies. *Ecol. Indic.* **2018**, *93*, 899–916. [[CrossRef](#)]
24. Golzio, A. High-Mountain Environment under Climate Change, the Interactions between Climate, Meteorology and Geomorphological Factors. Ph.D. Thesis, Università degli Studi di Milano, Milano, Italy, 2020. [[CrossRef](#)]
25. Bertolotto, P.L.; Mercalli, L.; Cat Berro, D.; Mosello, R.; Rogora, M. La serie climatica ultracentenaria di Domodossola Collegio Rosmini, 1871-2013. *Nimbus* **2014**, *XXII*, 4–45.
26. Cat Berro, D.; Mercalli, L.; Bertolotto, P.L.; Mosello, R.; Rogora, M.; Orrù, A. Il clima dell'Ossola Superiore. *Nimbus* **2014**, *XXII*, 46–129.
27. Hantke, R. The formation of the valleys between Domodossola and Locarno: Ossola Valley, Viguzzo Valley (Novara province) and Centovalli (Canton Ticino). *Boll. Soc. Ticin. Sci. Nat.* **1988**, *76*, 123–139.
28. Luciani, M. *Piano Di Emergenza Di Protezione Civile Del Comune di Varzo—VB*; Comune di Varzo, Varzo, 2006.
29. Steck, A.; Della Torre, F.; Keller, F.; Pfeifer, H.R.; Hunziker, J.; Masson, H. Tectonics of the Lepontine Alps: Ductile thrusting and folding in the deepest tectonic levels of the Central Alps. *Swiss J. Geosci.* **2013**, *106*, 427–450. [[CrossRef](#)]
30. Maxelon, M.; Mancktelow, N.S. Three-dimensional geometry and tectonostratigraphy of the Pennine zone, Central Alps, Switzerland and Northern Italy. *Earth-Sci. Rev.* **2005**, *71*, 171–227. [[CrossRef](#)]
31. Stampfli, G.M.; Borel, G.D.; Marchant, R.; Mosar, J. Western Alps geological constraints on western Tethyan reconstructions. *J. Virtual Explor.* **2002**, *8*, 77. [[CrossRef](#)]
32. Matasci, B.; Epard, J.L.; Masson, H. The Teggiolo zone: A key to the Helvetic–Penninic connection (stratigraphy and tectonics in the Val Bavona, Ticino, Central Alps). *Swiss J. Geosci.* **2011**, *104*, 257. [[CrossRef](#)]
33. Spring, L.; Reymond, B.; Masson, H.; Steck, A. La nappe du Lebendum entre Alte Kaserne et le Val Cairasca (massif du Simplon): Nouvelles observations et interprétations. *Eclogae Geol. Helv.* **1992**, *85*, 85–104.
34. Clark, P.U.; Dyke, A.S.; Shakun, J.D.; Carlson, A.E.; Clark, J.; Wohlfarth, B.; Mitrovica, J.X.; Hostetler, S.W.; McCabe, A.M. The Last Glacial Maximum. *Science* **2009**, *325*, 710–714. [[CrossRef](#)]
35. Braakhekke, J.; Ivy-Ochs, S.; Monegato, G.; Gianotti, F.; Martin, S.; Casale, S.; Christl, M. Timing and flow pattern of the Orta Glacier (European Alps) during the Last Glacial Maximum. *Boreas* **2020**. [[CrossRef](#)]
36. Rigamonti, I.; Uggeri, A. L'evoluzione dell'Alpe Veglia nel quadro delle Alpe Centrali. *Geol. Insubrica* **2016**, *1*, 69–83.
37. Sacco, F. *Il Glacialismo nelle Valli Sesia, Strona, Anza e Nell'ossola*; Ministero dei Lavori Pubblici—Servizio Idrografico—Ufficio Idrografico del Po: Roma, Italy, 1930; 106p.
38. Bollati, I.M.; Crosa Lenz, B.; Caironi, V. A multidisciplinary approach for physical landscape analysis: Scientific value and risk of degradation of outstanding landforms in the glacial plateau of the Loana Valley (Central-Western Italian Alps). *Ital. J. Geosci.* **2020**, *139*, 1–18. [[CrossRef](#)]
39. Gandini, D.; Muraro, M.; Paesano, G.; Pelosini, R. *Eventi Alluvionali in Piemonte, Chap 1: Analisi Meteorologica ed Idrologica*; ARPA Piemonte: Torino, Italy, 2003.
40. Cavalli, M.; Trevisani, S.; Comiti, F.; Marchi, L. Geomorphometric assessment of spatial sediment connectivity in small Alpine catchments. *Geomorphology* **2013**, *188*, 31–41. [[CrossRef](#)]

41. Bollati, I.M.; Cavalli, M. Geomorphic systems, sediment connectivity and geomorphodiversity: Relations within a small mountain catchment in the Lepontine Alps. *Geomorphometry 2021* 2020, in press.
42. Trigila, A.; Iadanza, C.; Spizzichino, D. Quality assessment of the Italian Landslide Inventory using GIS processing. *Landslides* **2010**, *7*, 455–470. [[CrossRef](#)]
43. ISPRA. *Dissesto Idrogeologico in Italia: Pericolosità e Indicatori Di Rischio*; Technical Report ISPRA 287/2018; ISPRA: Roma, Italy, 2018.
44. Blahut, J.; Van Westen, C.J.; Sterlacchini, S. Analysis of landslide inventories for accurate prediction of debris-flow source areas. *Geomorphology* **2010**, *119*, 36–51. [[CrossRef](#)]
45. Golzio, A.; Bollati, I.M.; Ferrarese, S. An Assessment of Coordinate Rotation Methods in Sonic Anemometer Measurements of Turbulent Fluxes over Complex Mountainous Terrain. *Atmosphere* **2019**, *10*, 324. [[CrossRef](#)]
46. Copernicus Climate Change Service (C3S) 2017 ERA5: Fifth Generation of ECMWF Atmospheric Reanalyses of the Global Climate. Copernicus Climate Change Service Climate Data Store (CDS). Available online: <https://cds.climate.copernicus.eu/cdsapp#!/home> (accessed on 8 January 2020).
47. NASA-JPL. NASA Shuttle Radar Topography Mission Global 3 arc-second [data set]. NASA EOSDIS Land Processes DAAC. *Tech. Rep.* **2013**. [[CrossRef](#)]
48. Büttner, G.; Soukup, T.; Kosztra, B. *CLC2012 Addendum to CLC2006 Technical Guidelines*; Technical Report; European Environmental Agency: Wien, Austria, 2013.
49. Hong, S.-Y.; Lim, J.-O.J. The WRF single-moment 6-class microphysics scheme (WSM6). *J. Korean Meteor. Soc.* **2006**, *42*, 129–151.
50. Dudhia, J. Numerical study of convection observed during the Winter Monsoon Experiment using a mesoscale two-dimensional model. *J. Atmos. Sci.* **1989**, *46*, 3077–3107. [[CrossRef](#)]
51. Mlawer, E.J.; Taubman, S.J.; Brown, P.D.; Iacono, M.J.; Clough, S.A. Radiative transfer for inhomogeneous atmospheres: RRTM, a validated correlated-k model for the longwave. *J. Geophys. Res.* **1997**, *102*, 16663–16682. [[CrossRef](#)]
52. Jiménez, P.A.; Dudhia, J. Improving the representation of resolved and unresolved topographic effects on surface wind in the WRF model. *J. Appl. Meteorol. Climatol.* **2012**, *51*, 300–316. [[CrossRef](#)]
53. Tewari, M.; Chen, F.; Wang, W.; Dudhia, J.; LeMone, M.A.; Mitchell, K.; Ek, M.; Gayno, G.; Wegiel, J.; Cuenca, R.H. Implementation and verification of the unified NOAA land surface model in the WRF model. In Proceedings of the 20th Conference on Weather Analysis and Forecasting/16th Conference on Numerical Weather Prediction, Seattle, WA, USA, 12–16 January 2004; pp. 11–15.
54. Hong, S.-Y.; Noh, Y.; Dudhia, J. A new vertical diffusion package with an explicit treatment of entrainment processes. *Mon. Wea. Rev.* **2006**, *134*, 2318–2341. [[CrossRef](#)]
55. Grell, G.A.; Freitas, S.R. A scale and aerosol aware stochastic convective parameterization for weather and air quality modeling. *Atmos. Chem. Phys.* **2014**, *14*, 5233–5250. [[CrossRef](#)]
56. Colombo, A.; Ramasco, M. Analisi del dissesto da frana in Piemonte. Rapporto sulle frane in Italia. *ISPRA* **2007**, *78*, 81–120.
57. Cruden, D.M.; Varnes, D.J. Landslides: Investigation and mitigation. Chapter 3-Landslide types and processes. *Transp. Res. Board Spec. Rep.* **1996**, *247*, 36–75.
58. Tropeano, D.; Turconi, L. Alluvione del 14-15 ottobre 2000 nell'Italia del nord-ovest: Cronaca di sintesi e commenti. *Nimbu* **2001**, *21–22*, 53–85.
59. Luino, F.; De Graff, J.V.; Roccati, A.; Biddoccu, M.; Cirio, C.G.; Faccini, F.; Turconi, L. Eighty Years of Data Collected for the Determination of Rainfall Threshold Triggering Shallow Landslides and Mud-Debris Flows in the Alps. *Water* **2019**, *12*, 133. [[CrossRef](#)]
60. Giordan, D.; Manconi, A.; Allasia, P.; Bertolo, D. Brief Communication: On the rapid and efficient monitoring results dissemination in landslide emergency scenarios: The Mont de La Saxe case study. *Nat. Hazards Earth Syst. Sci.* **2015**, *15*, 2009–2017. [[CrossRef](#)]

